JOURNAL OF THERMOPHYSICS AND HEAT TRANSFER
Vol. 23, No. 3, July–September 2009

Thermal Aspects of Satellite Downscaling

H. van Weeren,* H. J. M. ter Brake,† and G. Holl‡
University of Twente, Enschede, 7500 AE Enschede, The Netherlands
R. J. Hamann§
Delft University of Technology, 2600 AA Delft, The Netherlands
and
S. Price¶
Astrium UK, Stevenage, England SG1 2AS, United Kingdom

DOI: 10.2514/1.41857

The strong trend toward nanosatellites creates new challenges in terms of thermal balance control. The thermal balance of a satellite is determined by the heat dissipation in its subsystems and by the thermal connections between them. As satellites become smaller, heat dissipation in their subsystems tends to decrease and thermal connectivity scales down with dimension. However, these two terms do not necessarily scale in the same way, and so the thermal balance may alter and the temperature of subsystems may reach undesired levels. This paper focuses on low-Earth-orbit satellites. We constructed a generalized lumped thermal model that combines a generalized low-Earth-orbit satellite configuration with scaling trends in subsystem heat dissipation and thermal connectivity. Using satellite mass as a scaling parameter, we show that subsystems do not become thermally critical by scaling mass alone.

Nomenclature

A_{ij}	=	interface contact area between i and j
A_p	=	body panel area
C_{battery}	=	battery capacity
F_{ij}	=	view factor between i and j
GL_{ij}	=	conduction constant between i and j
GR_{ij}	=	radiation constant between i and j
h	=	heat transfer coefficient
L_{char}	=	characteristic length of the satellite
l	=	length of thermal path
m	=	satellite mass
P_{ij}	=	electrical power or work
Q_{ij}	=	heat flow from i to j
q_i	=	heat flux
T	=	temperature
$T_{\max}$	=	maximum subsystem operating temperature
$T_{\min}$	=	minimum subsystem operating temperature
V	=	satellite body volume
α	=	solar absorptance
ε	=	emmisivity
λ	=	thermal conductivity
η	=	subsystem efficiency
σ	=	Stefan–Boltzmann constant
τ_{eclipse}	=	time in eclipse

Subscripts

A	=	albedo
B	=	background or deep space
E	=	Earth
env	=	environment
i, j	=	objects accounted for in the analysis
S	=	sun
$-X$	=	$-X$ body panel
$+X$	=	$+X$ body panel
$-Y$	=	$-Y$ body panel
$+Y$	=	$+Y$ body panel
$-Z$	=	$-Z$ body panel
$+Z$	=	$+Z$ body panel

Received 28 October 2008; accepted for publication 7 February 2009.

*Research Fellow, Low Temperatures Division/Cooling and Instrumentation Group.
†Professor, Low Temperatures Division/Cooling and Instrumentation Group; h.j.m.terbrake@utwente.nl.
‡BSc. Student, Low Temperatures Division/Cooling and Instrumentation Group.
§Senior Lecturer, Chair of Space Systems Engineering; r.j.hamann@lr.tudelft.nl.
¶Head of the Thermal Analysis Group; steve.price@astrium.eads.net.

I. Introduction

SMALL nanosatellites weighing 1–10 kg have several advantages over larger satellites. First, they can be piggyback-launched in the spare space of a vehicle that carries a larger payload. The resulting cost reduction is especially interesting for technology demonstrators that are developed in the academia. Second, several of them may be launched as a colony that orbits in formation. This configuration offers a high level of redundancy, because the functionality of a damaged satellite can be taken over by the others. Moreover, a constellation of nanosatellites can observe a larger area (for instance, of the Earth) than a single normal-sized satellite. Examples of nanosatellites are Delfi C^3 [1] and the CanX family [2].** These satellites are typical examples of technology demonstrators developed at universities.

The thermal balance of a satellite is determined by the thermal coupling with its environment (Earth, albedo, and sun), by the thermal couplings between its subsystems, and by the heat dissipated in active subsystems. Radiative coupling scales with the surface area A, and conductive coupling is proportional to A/l, where A is the cross-sectional area and l is the length of the thermal path. Dissipation in active subsystems scales with their power consumption and with their inefficiency. Clearly, as satellites become smaller radiative, conductive and dissipative terms do not necessarily scale in the same way and the thermal balance may change. As a consequence, subsystems may become thermally critical (i.e., their operating temperature can reach undesired levels).

Focusing on low-Earth orbit (LEO) satellites, this study analyzes how their thermal balance alters with downscaling and which of their subsystems become thermally critical. Our analysis is based on

**Data available online at http://www.delfic3.nl and http://www.utias-sfl.net/ [retrieved 7 April 2009].

scaling trends of real data of satellites in a wide range of dimensions. Therefore, our thermal analysis also takes into account engineering decisions and clearly reveals whether currently available technology hampers downscaling. Although we limit ourselves in this paper to LEO satellites, the method used can also be applied for other (Earth observation) satellite missions.

This paper is organized as follows: Sec. II presents the assumptions that are used to arrive at a generalized LEO satellite model, together with typical LEO parameters. Section III discusses typical thermal requirements of LEO satellite subsystems so that statements can be made whether or not they become thermally critical. Section IV treats scaling trends in the heat dissipation within subsystems, and Sec. V analyzes the scaling behavior of thermal connections. The overall lumped thermal model of the generalized LEO satellite is presented in Sec. VI. Finally, Sec. VII presents the results of the thermal analysis, showing how subsystem heat fluxes and temperatures tend to scale with satellite size. Included in this section is a sensitivity analysis that gauges how alternative LEO parameters, internal thermal couplings and scaling trends tend to affect the thermal balance of a satellite and how this influences the outcome of this study.

II. Model Satellite

The thermal network of a satellite is based on its thermal coupling with the environment and on the internal couplings between subsystems. The thermal coupling with the environment depends on the orbit parameters, on the shape of the satellite, and on the properties of its surface. This scaling study assumes a generalized satellite body shape as well as a typical orbit and surface, all of which are presented in Sec. II.A. Section II.B defines a generalized internal satellite configuration that will be used to determine the internal thermal balance. Section II.C discusses the relationship between satellite mass and dimensions. This is important because we use the satellite mass as a scaling parameter, whereas thermal couplings tend to scale with dimensions.

A. Generalized LEO Satellite and Orbit Parameters

The shape of a satellite obviously depends on its functionality. However, for this scaling study, we assume an Earth observation mission and take a cube as the generalized body shape. Each body panel has a different functionality, as shown in Fig. 1a. The $-Z$ panel points toward the nadir and contains the sensors for Earth observation. The $-Y$ panel, containing the electrical-power-providing solar array, points in the direction of motion. Finally, radiators are placed on the $-X$ and $+X$ panels to transmit internally dissipated heat to the environment.

Table 1 Typical low-Earth-orbit properties

Orbit	Sun-synchronous
Altitude, km	700
Inclination, deg	98.2
Ascending node, deg	37.5
Orbit time, min	100
Sunlit, min	60
Solar flux, W/m^2	1370
Albedo fraction, %	30
Earth flux, W/m^2	236

The orbit of the model satellite is assumed to be a low Earth orbit. Typical LEO orbits are sun-synchronous and have altitudes ranging between 400 and 800 km. The orbit properties chosen for this study are listed in Table 1. They represent average values of a range of LEO missions, inventoried in Table 2. The orientation of the satellite along its orbit is shown in Fig. 1b. The effect of the orbit parameters on the results of our analysis is considered in Sec. VII.B.

Because this study seeks to analyze the *general* effect of system scaling on subsystem temperatures, we average the thermal balance between the satellite and its environment over the orbit and neglect transient effects due to transitions between eclipse and sunlit periods.

B. Internal Satellite Configuration

To estimate the internal thermal balance of the model LEO satellite, we need to define typical subsystems and their interconnections. Just like the body shape, satellite subsystems vary according to the satellite's functionality. From a thermal point of view, however, LEO satellite subsystems can be generalized fairly well, as indicated in Fig. 2. The typical active subsystems that dissipate heat are the power supply (PS), the communication unit (CU), the attitude control (AC), and the payload (PL). Note that for the internal thermal balance, we neglect transient effects (e.g., due to the on- and offswitching of subsystems.

The power supply consists of a solar array, batteries, charge, discharge regulators, and a bus regulator. During the sunlit period, the solar array powers the subsystems but also charges the batteries. In this period, dissipation within the PS mainly occurs in the charge regulators, in the charging batteries, and in the bus regulator. During eclipse, the batteries provide power to the subsystems, and PS dissipation is found in the discharge regulators and in the discharging battery.

The communication unit provides command and data transmission to and from the ground segment. The main dissipating element in the CU is its amplifier. Amplifiers in satellite CUs are

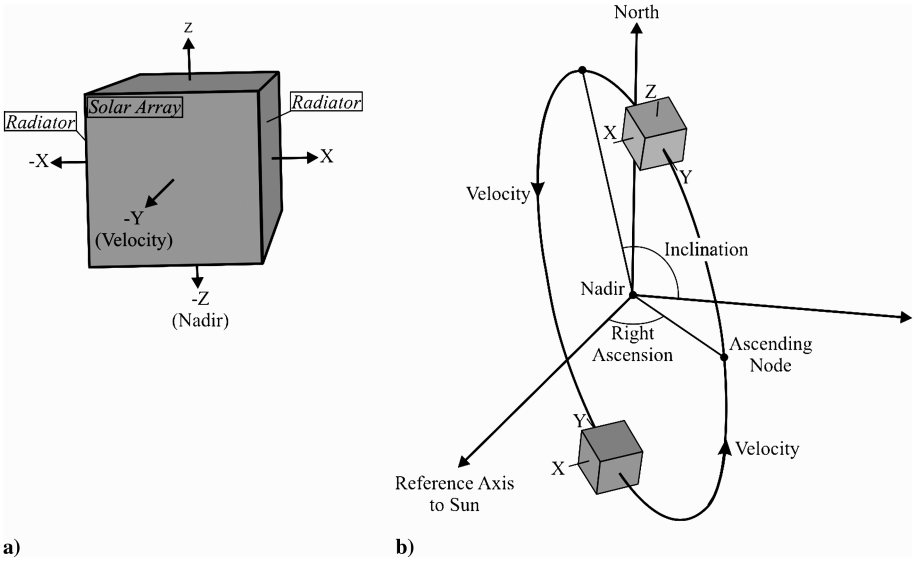

Fig. 1 Illustrations of a) the generalized model satellite and b) an overview of the model satellite in its orbit.

Table 2 Overview of LEO/sun-synchronous missions that are included in the trends

Mission	Inclination, deg	Altitude, km	Orbit time, min	Mass, kg	Volume, m^3	Power budget, W	Ref.[a]
EnviSAT	98.00	800	101	8200	1.74×10^2	3300	ESA
MetOp	98.70	817	101	4093	7.17×10^1	1812	ESA
ALOS	98.16	692	——	4000	9.36×10^1	7000	ESA
ERS2	98.50	800	100	2516	1.75×10^2	——	ESA
ERS1	98.50	800	100	2384	1.75×10^2	2600	ESA
JERS-1	98.00	570	96	1400	5.58×10^0	——	ESA
IRS-P6	98.70	817	101	1360	——	1250	ESA, ISRO
EarthCARE	——	450	——	1238	——	1068	ESA
IRS-P4	98.28	720	99	1050	1.42×10^2	750	ISRO
GOCE	96.50	250	——	1000	5.00×10^0	1300	ESA
QuikSCAT	——	——	——	970	——	874	ESA
Nimbus-7	99.10	955	104	965	5.52×10^0	——	ESA
IRS-P3	98.68	817	——	920	——	817	ESA, ISRO
SMOS	98.40	763	——	683	9.97×10^0	900	FNSA
ADM-Aeolus	97.00	408	——	650	1.75×10^1	1400	ESA
Kompsat-1	98.13	685	98	510	3.24×10^0	630	ESA
Odin	——	600	——	250	2.42×10^0	340	ESA
Proba	97.90	600	5818	94	2.88×10^{-1}	120	ESA
HAMSAT	97.80	632	——	43	2.50×10^{-1}	——	[3]
CanX-2	——	——	——	4	3.40×10^{-3}	——	[2]
Delfi C^3	98.00	600	97	3	3.40×10^{-3}	3	——

[a]ESA denotes the European Space Agency, ISRO denotes the Indian Space Research Organization, and FNSA denotes the French National Space Agency.

usually solid-state power amplifiers (SSPAs) or traveling-wave tube amplifiers (TWTAs).

The attitude control maintains the attitude and orbit of the satellite. Typical attitude control actuators are thrusters, magnetic torquers, momentum wheels, reaction wheels, and control moment gyros. The most common AC components in LEO (and other small) satellites are reaction wheels and magnetic torquers.

The payload contains the mission-specific subsystems. In our generalized thermal model, PL subsystems are the receiver unit, which performs the actual observation, and the normal-temperature unit containing the processing electronics. Here, normal temperature is defined as the operating temperature of the satellite. Optionally, there is also a low-temperature unit containing electronic components that operate at temperatures well below the normal level. A heat pump is connected to the low-temperature unit to cool these components. Because the PL does not perform any work on its environment, power dissipation within the PL is equal to its input power.

For the thermal couplings, we assume that all subsystems are thermally connected to a central heat sink (HS), through which heat is rejected to deep space by a radiator. Note that the subsystem positioning depicted in Fig. 2 is not necessarily representative for actual satellite configurations. Positioning is dictated by the allocation of the available panel area to the footprints of the various subsystems and will be discussed further in Sec. V.

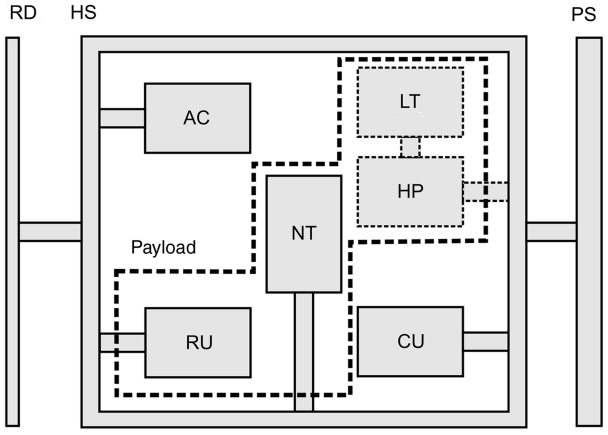

Fig. 2 Generalized thermal system of a LEO Earth-observing satellite. PS is the power supply, CU is the communication unit, RU is the receiver unit, NT is the normal-temperature unit, LT is a low-temperature unit cooled by a heat pump (HP), AC is the attitude control, HS is the heat sink, and RD is the radiator.

C. Mass Versus Dimensions of Satellites

Because the commonly used terms pico-, nano, and microsatellite refer to a satellite's mass rather than to its dimensions, this study uses mass as a scaling parameter. However, thermal couplings depend on (geometrical) size, and so a relation is needed between mass and size. To establish a general trend, the volumes and masses of the LEO satellites listed in Table 2 are plotted against each other in Fig. 3.

Note that the body volume plotted in Fig. 3 corresponds to the undeployed state and thus excludes the dimensions of extremities such as antennas and deployable solar arrays. The resulting trend line is

$$V = 4 \times 10^{-4} \cdot m^{1.5824} \tag{1}$$

where the satellite body volume V is expressed in cubic meters and its mass m is expressed in kilograms. The fit has an R^2 value of 0.96. Because our model satellite is cubic, a generalized characteristic length L_{char} is straightforwardly defined as

$$L_{\text{char}} \equiv V^{1/3} = 73.6 \times 10^{-3} \cdot m^{0.5274} \tag{2}$$

where L_{char} is expressed in meters.

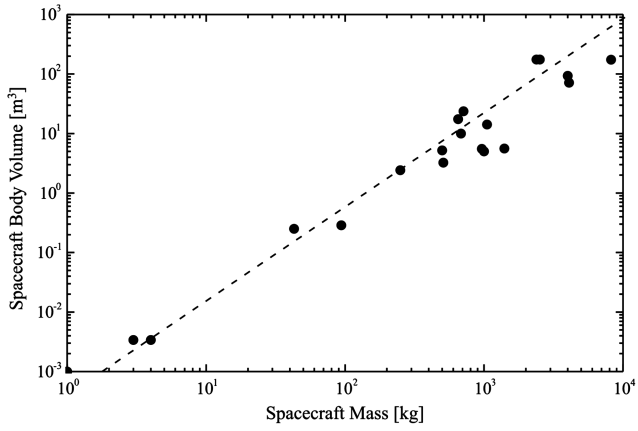

Fig. 3 Spacecraft body volume as a function of the spacecraft mass.

Table 3 Typical subsystem operating temperatures

	PS		CU		AC		PL		
Mission	T_{min}, °C	T_{max}, °C	T_{min}, °C	T_{max}, °C	T_{min}, °C	T_{max}, °C	T_{min}, °C	T_{max}, °C	Ref.
SPOT-1	−5	20	−20	70	−25	55	−10	50	[4]
OTS	−20	30	−10	47	−10	45	——	——	[4]
LandSAT-D	——	——	−4	30	——	——	10	30	[4]
Delfi C^3	——	——	−40	85	——	——	−40	80	——
ERS-1	−15	40	——	——	——	——	−10	40	[5]
HAMSAT	10	30	——	——	——	——	0	40	[3]
Average	−8	30	−19	58	−18	50	−10	48	——

III. Thermal Requirements of Subsystems

Whether or not a subsystem becomes thermally critical depends on its actual components. For example, as mentioned in Sec. II.B, there are different choices for AC actuators, each with its own thermal requirements. To determine if the subsystems in our generalized thermal model fulfill these requirements, we derive typical operating temperature ranges of subsystems by averaging collected data on specific satellites (Table 3). For safe operation, the temperature of the subsystems in our model satellite should fall within the averaged-temperature window.

IV. Scaling of the Subsystem Heat Dissipation

Figure 4 shows the overall power budget of the satellites listed in Table 2 plotted against their mass, including the 85% prediction band.

A relation between power and mass can be established as

$$P_{S/C} = 1.54 \cdot m^{0.9328} \tag{3}$$

where m is the mass in kilograms and $P_{s/c}$ is the power budget in watts. The R^2 value of this fit is 0.90.

Figure 5 shows the trend lines for the power consumption of the individual subsystems [6] along with the overall power budget trend given by Eq. (3). Note that the scaling trends of the subsystems found in [6] range up to about 2000 kg. As such, we set the upper limit of our analysis at 1000 kg. As discussed in Sec. II.B, the power supply itself also consumes power and is therefore included in the figure as a separate subsystem.

The solid lines illustrate how the subsystems of heavier spacecraft ($m \geq$ 50–100 kg) each take up a more or less fixed percentage of the overall power budget. However, this proportionality no longer holds for lighter spacecraft, in which subsystem power consumption tends to level off at a constant value. Considering the CU, for instance, the lower limit of about 10–20 W is dictated by the minimum amount of RF output power that is required for data transfer to the ground segment. Clearly, further scaling down of satellites in such a way that the power consumption of their subsystems also reduces requires technology changes. The development of Delfi-C^3, in which increased efficiency results in a CU power consumption of only 1.8 W, reflects such a technology change. Further examples of power-efficient subsystem miniaturization are the development of thrusters at the Netherlands Organization for Applied Scientific Research [7][††] and reaction wheels at Technische Universität Berlin [8].[‡‡] Both developments aim at physical miniaturization as well as power consumption reduction of the AC in CubeSats. Roughly extrapolating from these examples, it can be expected that similar power-efficient technologies will also be developed for the other subsystems. In the remainder of our thermal analysis, we will therefore assume that the power consumption for all subsystems remains at a fixed percentage of the overall budget. These prospected trend lines are indicated by the dashed lines in Fig. 5.

The electrical power allocated to the PS and to the PL is completely converted into heat. This is not the case for the CU and for the AC: the CU provides work in terms of RF output power and the AC applies a satellite torque. To determine the heat dissipated in these subsystems, their efficiency needs to be estimated.

Starting with the CU, the observed efficiency of TWTAs and SSPAs depends strongly on the RF output power, as shown in Fig. 6. TWTAs are generally significantly more efficient than SSPAs. Nevertheless, the lower operating voltage of SSPAs tends to make them more reliable than TWTAs, and so they are preferred up to RF output powers of 10 W. As mentioned already, the SSPA in Delfi C^3, with an efficiency of 12.5% at 0.2 W RF output power, breaks with the observed trend shown in Fig. 6. This illustrates how technology

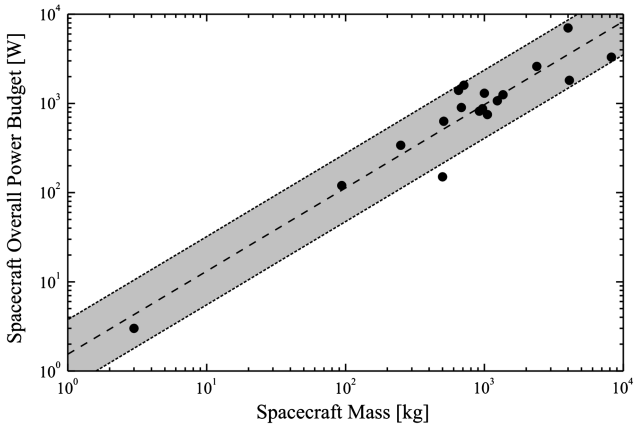

Fig. 4 Overall spacecraft power budget versus the spacecraft mass (Table 2). The gray band indicates the 85% prediction band.

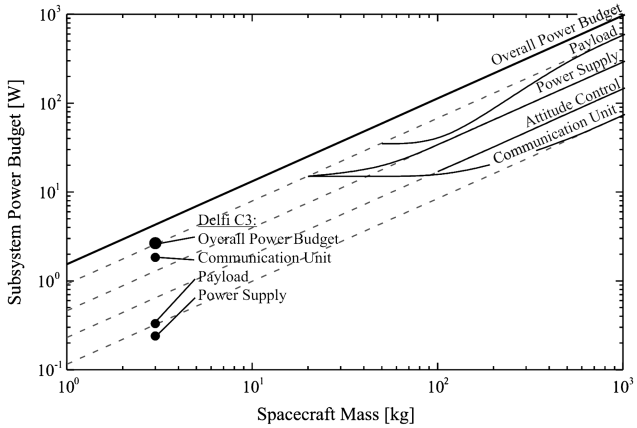

Fig. 5 Observed trends in subsystem power budgets versus spacecraft mass (solid lines) [6]. The data points correspond to Delfi C^3. The gray dashed lines indicate prospected trends, taking into account technology changes (see Sec. IV).

[††]This development is in cooperation with the Delft University of Technology and the University of Twente within the framework of the Dutch MicroNed program.

[‡‡]This development is within the framework of the development of the BeeSat satellite (data available online at http://www.BeeSat.de [retrieved 7 April 2009]).

Table 4 Absorbed average heat influx from the sun (q_S), albedo (q_A), and Earth (q_E) and the overall absorbed influx

Body panel	q_S, W/m^2	q_A, W/m^2	q_E, W/m^2	Total absorbed influx, W/m^2
$+Z$	107.1	0.0	0.0	$Q_{\text{env},+Z}/A_p = 107.1$
$-Z$	28.7	25.7	19.9	$Q_{\text{env},-Z}/A_p = 74.3$
$+X$ radiator	67.1	3.4	47.8	$Q_{\text{env},+X}/A_p = 118.3$
$-X$ radiator	0.0	2.6	47.7	$Q_{\text{env},-X}/A_p = 50.3$
$+Y$	75.8	7.5	6.0	$Q_{\text{env},+Y}/A_p = 89.3$
$-Y$ solar array	184.4	18.2	48.0	$Q_{\text{env},-Y}/A_p = 250.3$

changes are expected to render SSPAs more efficient, and so we will assume that SSPAs are used throughout the satellite mass range.

The efficiency of ACs with reaction wheels is generally quite low: typically, only ~10% of their input power is actually used to apply torque to the spacecraft, and the remaining 90% of their power budget is dissipated as heat [6].

Combining the typical efficiencies of subsystems with their prospected power consumptions (the dashed lines in Fig. 5) allows estimating the scaling relations for their heat dissipation:

$$Q_{\text{PL}} = 0.924 \cdot m^{0.9328}$$

$$Q_{\text{PS}} = 0.462 \cdot m^{0.9328} \qquad Q_{\text{AC}} = 0.208 \cdot m^{0.9328}$$

$$Q_{\text{CU}} = [0.076 - 0.039 \cdot \exp(-1.78 \times 10^{-3} \cdot m^{0.9328})] \cdot m^{0.9328} \quad (4)$$

where Q is the heat dissipation in watts and m is the satellite mass in kilograms. Note that the form of the CU expression deviates from the others to take into account the RF output power dependence of the CU efficiency (Fig. 6).

V. Scaling the Thermal Connections

The next element in the analysis is the mass-scaling behavior of thermal connections. They can be separated into external connections with the environment and internal connections between subsystems. Environmental thermal connections are discussed in Sec. V.A, and internal connections are discussed in Sec. V.B.

A. Environmental Thermal Connections

Obviously, environmental thermal connections have a radiative nature. The *incoming* environmental heat flow $Q_{\text{env},i}$ on satellite panel i can be split into four separate terms:

$$Q_{\text{env},i} = Q_{S,i} + Q_{A,i} + Q_{E,i} + Q_{B,i} \quad (5)$$

The four terms on the right-hand side indicate incoming radiative heat flows from the sun, from the albedo, from the Earth infrared, and from the space background, respectively. The radiative heat flow *emitted* by the panel i can be expressed as

$$Q_{i,\text{env}} = \sigma \varepsilon_i A_i T_i^4 \quad (6)$$

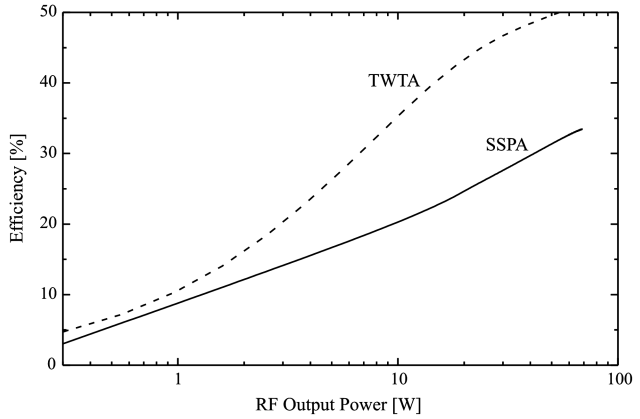

Fig. 6 Efficiency of the communication unit as a function of the RF output power [6].

where σ is the Stefan–Boltzmann constant, ε_i is the emissivity of the panel, A_i is its area, and T_i is its temperature. The value of T_i can be determined from a heat balance equation that includes the heat flow Q_i from the spacecraft components that are thermally linked to the panel. Neglecting the space background radiation $Q_{B,i}$, we write

$$Q_{S,i} + Q_{A,i} + Q_{E,i} + Q_i = \sigma \varepsilon_i A_i T_i^4 \quad (7)$$

The incoming environmental heat flux is evaluated using ESARAD [9] with orbit-averaged view factors. For the thermo-optical properties, it is assumed that the radiator body panels $-X$ and $+X$ have an emissivity and solar absorptance similar to that of optical solar reflectors ($\varepsilon = 0.83$ and $\alpha = 0.12$) [6], and the solar array on the $-Y$ panel has properties similar to Si ($\varepsilon = 0.82$ and $\alpha = 0.73$) [6]. For the other panels ($+Y$, $-Z$, and $+Z$), we averaged the emissivity and solar absorptance of commonly used materials ($\varepsilon = 0.1$ and $\alpha = 0.30$) [6]. Further (default) assumptions in ESARAD [9] are an averaged Earth temperature of -16°C and an Earth emissivity of 1.0. The resulting orbit-averaged heat fluxes from the environment to the body panels are listed in Table 4.

The calculated heat fluxes obviously scale with the body panel areas A_p. To relate heat flow with the mass of our cubic model satellite, A_p is taken to be the square of L_{char}. Using Eq. (2), A_p then relates to the satellite mass as

$$A_p \equiv L_{\text{char}}^2 = 5.43 \times 10^{-3} \cdot m^{1.06} \quad (8)$$

where A_p is expressed in square meters and m is in kilograms.

B. Internal Thermal Connections

1. Subsystems

Because highly conductive elements such as Al or Cu are relatively heavy and because heat pipes significantly complicate the thermal design, dissipating subsystems are usually bolted directly onto the radiator. A typical material used as thermal interface is Sigraflex,[§§] with a practical heat transfer coefficient of $h = 200$ W/m$^2 \cdot$K. A thermal path with an equal cross-sectional area and made up of Cu (400 W/m $\cdot$ K) would need to have a length exceeding 2 m to have a higher thermal resistance. Therefore, our scaling analysis assumes thermal couplings to be determined by the interface contact area and by the heat transfer coefficient h. The resulting conduction constant GL_{ij} is thus defined as

$$GL_{ij} = A_{ij} h \quad (9)$$

and the conductive heat flow is

$$Q_{ij} = GL_{ij} \cdot (T_i - T_j) \quad (10)$$

Assuming the value of $h = 200$ W/m^2 K for all subsystems, the interface area A_{ij} remains to be determined. Because the power density of the PL is typically less than those of the CU, the AC, and the PS, we assume that the latter three subsystems are mounted on the $-X$ radiator. The remaining area available on the $-X$ and $+X$ radiators is allocated to the PL.

The footprint of the CU [i.e., the SSPA (see Sec. IV)] does not show a clear trend with its RF output power. CUs are typically purchased from external suppliers and their size varies from one

[§§]Data available online at http://www.sglcarbon.com/sgl_t/expanded/innovative/electronics.html [retrieved 7 April 2009].

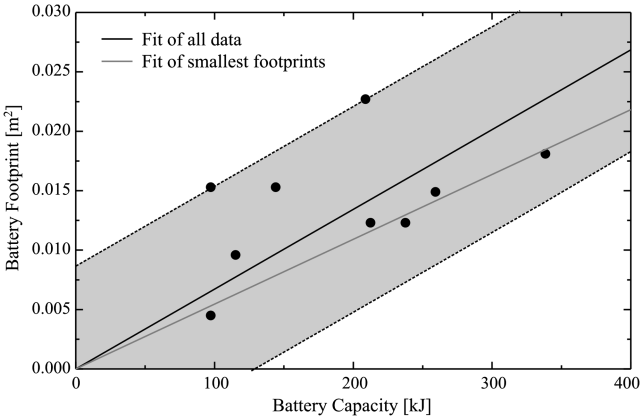

Fig. 7 Battery pack footprint versus capacity. The black line indicates the trend given in Eq. (11) while the gray line follows Eq. (12). The gray band is the 85% prediction band. The data are those of Li-Ion batteries of Dell laptops.

manufacturer to another. Moreover, to provide redundancy, some suppliers deliver CUs that contain two SSPAs. Nevertheless, we can generally take the footprint of CUs to be typically around $A_{CU-X} = 10 \times 15$ cm^2, independent of satellite mass. We furthermore assume the same footprint A_{AC-X} for the AC system.

As discussed in Sec. IV, there is a clear relationship between a satellite's overall power budget and its mass. Consequently, the capacity of the battery pack will also scale with the satellite mass. Although the PS also contains regulation electronics, the size of the battery pack usually dominates, and so we may take the PS footprint to be equal to the battery footprint. The footprints of several Li-ion batteries are plotted against their capacities in Fig. 7.

As indicated by the 85% prediction band, the data in Fig. 7 are considerably scattered. In our thermal analysis, we assume the solid black trend line, which represents a linear fit to all the data points:

$$A_{PS-X} = 6.7 \times 10^{-8} \cdot C_{battery} \tag{11}$$

where A_{PS-X} is expressed in square meters and $C_{battery}$ is in Joules. As part of the sensitivity analysis presented in Sec. VII.B, we will also use the gray trend line. This trend line corresponds to the batteries with the smallest footprints and might better represent the tendency to use smaller components for small satellites:

$$A_{PS-X} = 5.5 \times 10^{-8} \cdot C_{battery} \tag{12}$$

Assuming that the battery pack needs to deliver a power $P_{S/C} - P_{PS}$ to the satellite subsystems during the eclipse period $\tau_{eclipse} = 40$ min, and using Eqs. (3) and (4), the battery-pack footprint can be related to the satellite mass:

$$A_{PS-X} = c \cdot \tau_{eclipse} \cdot (P_{S/C} - P_{PS}) \tag{13}$$

where $c = 6.7 \times 10^{-8}$ or 5.5×10^{-8} m^2/J, corresponding to Eqs. (11) and (12), respectively. As mentioned already, the remaining area of the $-X$ radiator and the area of the $+X$ radiator are allocated to the PL. Assuming the two radiator panels to have equal area A_p and the payload to use the whole available area, the PL footprint becomes

$$A_{PL-X} = A_P - A_{PS-X} - A_{CU-X} - A_{AC-X} \quad \text{and} \quad A_{PL+X} = A_P \tag{14}$$

The heat fluxes from the payload to the $-X$ and $+X$ radiators are assumed to be equal (i.e., they result in the same ΔT at equal contact resistance), and so

$$\frac{Q_{PL-X}}{A_{PL-X}} = \frac{Q_{PL+X}}{A_{PL+X}} \tag{15}$$

where

$$Q_{PL} = Q_{PL-X} + Q_{PL+X}$$

The conduction constants GL_{PL-X}, GL_{PL+X}, GL_{CU-X}, GL_{AC-X}, and GL_{PS-X} can now be determined with the aid of Eq. (9).

2. Body Panels

Although the outer faces of the body panels have different thermo-optical properties corresponding to their different functionality, all inner panel faces are usually painted black to enhance internal radiative coupling. Once more, ESARAD [9] is used to calculate the effective thermal couplings GR_{ij} between the body panels. Normalized over area, the coupling constants between all body panel combinations turn out to be equal and are given by

$$\frac{GR_{ij}}{A_p} = 0.17 \tag{16}$$

Note that this expression neglects shadowing effects of the components that are mounted on the panels, as well as the coupling between them. Component coupling is considered in Sec. VII.B. Using Eq. (8), these radiative coupling constants are directly related to the satellite mass.

VI. Lumped Thermal Model

The lumped thermal network of the model satellite is shown in Fig. 8. In this model, the satellite subsystems and the body panels are the nodes of which the temperatures are solved by balancing the heat fluxes through the thermal couplings. To have a clear picture, the mutual radiative coupling between the panels, as discussed in the previous section, is not depicted in this figure.

Note that this lumped model differs from Fig. 2 in the sense that the central heat sink (i.e., the satellite body) is now separated into 6 body panels. In Table 4, each panel was shown to have a different thermal connection to the satellite's environment, and the previous section discussed how the PL is distributed over the $-X$ and $+X$ radiators.

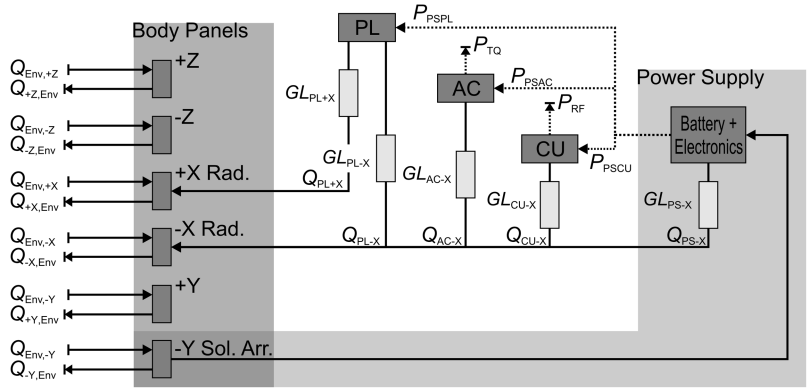

Fig. 8 Lumped thermal network of the model satellite (radiative coupling between panels is not included in the picture).

The heat dissipation in the various subsystems was given in Eq. (4) and results here in the heat fluxes Q_{ij}, with the subscript i referring to a subsystem and j referring to a radiator panel. The corresponding conductive coupling constants GL_{ij} were determined in Sec. V.B. The influx $Q_{\text{env }j}$ from the environment to each of the body panels is given in Table 4. Heat fluxes $Q_{j\text{ env}}$ from the body panels to the environment depend on the panel's temperature and follow from the heat balance of the whole satellite.

VII. Results

The mass-scaling trends discussed in Secs. II, III, IV, and V, together with the thermal network described in Sec. VI, are entered into the software package ThermXL [10], for which the solver is then executed for several values of satellite mass. The temperatures of the nodes (i.e., the subsystems and the body panels) as well as the heat fluxes between them are the output of the model calculations. The mass-scaling behavior of these subsystem temperatures and heat fluxes is discussed in Sec. VII.A. In Sec. VII.B, a sensitivity analysis is performed in which the influence of alternative orbit parameters, of radiative cross-couplings between subsystems, and of the battery footprint is studied.

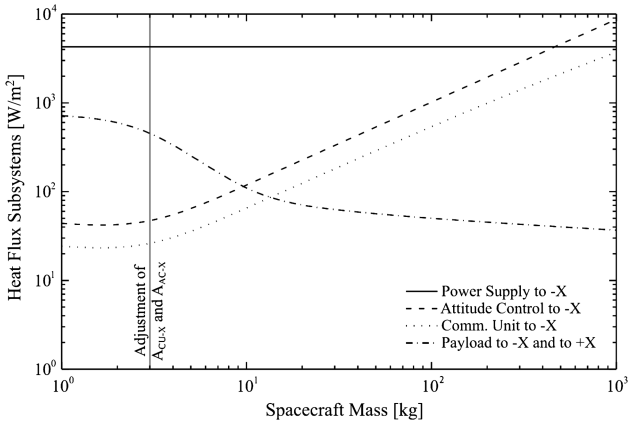

Fig. 9 Dissipative heat fluxes from the subsystems to the radiator panels.

A. Standard Orbit Calculations

Figure 9 shows the heat fluxes from the subsystems to the radiator panels (i.e., the heat dissipated in a subsystem divided by its footprint) plotted against satellite mass. Heat fluxes from the environment are not plotted, because they do not depend on the mass (Table 4). Heat fluxes between panels are constant as well, and so the only mass-dependent heat fluxes are those due to subsystem dissipation. This directly implies that any mass dependence of a subsystem's temperature is dictated by the mass dependence of its heat dissipation.

As shown in Fig. 9 and directly derived from Eq. (11), the dissipative heat flux from the PS is constant. Note also that the heat fluxes from the PL to the $-X$ and $+X$ panels are equal, as follows from Eq. (15).

Because the footprint of both the CU and the AC are assumed to be constant, their dissipative heat fluxes to the radiator panel are almost linearly dependent on mass, corresponding to Eq. (4). However, this nearly linear dependence ceases to be valid below $\sim$3 kg. Below this mass, the satellite is too small to accommodate the footprint of the AC and CU. Their footprints are therefore adjusted from 150 down to 50 cm^2. This also affects the heat flux from the PL, because its footprint is determined by the remaining available area on the radiators. Note that the assumed reduction in CU and AC footprints

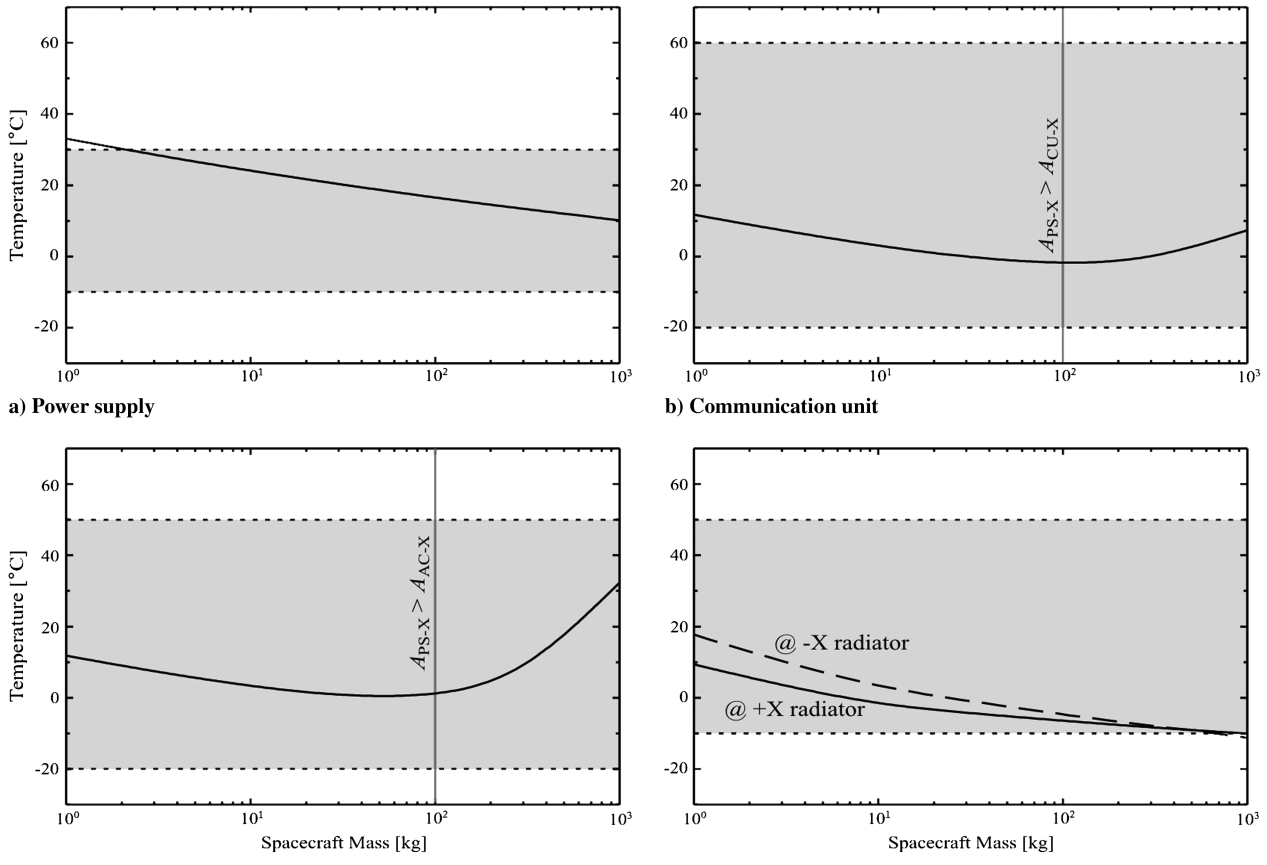

Fig. 10 Temperatures of the subsystems as a function of the satellite mass. The gray band indicates the temperatures in which the subsystem temperatures tend to fall.

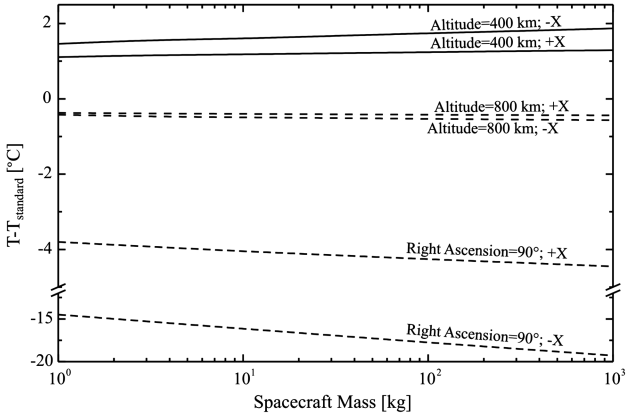

Fig. 11 Changes in subsystem temperature for orbit parameters other than standard parameters (see Table 1) plotted against satellite mass.

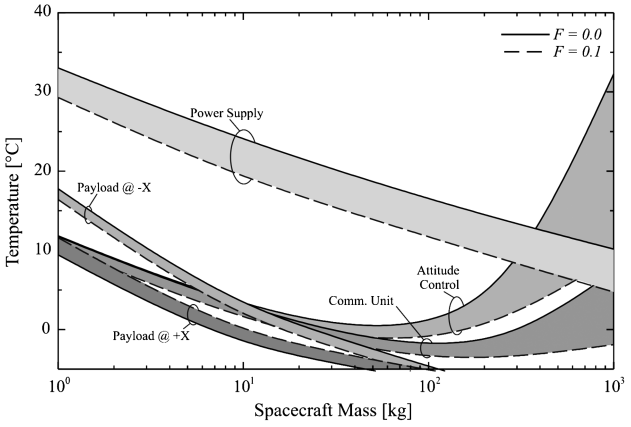

Fig. 12 Influence of radiative couplings between subsystem temperatures on their temperature.

implies a technology change that is mandatory for further downscaling.

Subsystem temperatures follow from the heat fluxes and are plotted in Fig. 10. When the satellite is scaled down from 1000 to 100 kg, the AC and CU temperatures tend to decrease, reflecting the decrease in their heat fluxes. Below ∼100 kg, however, their temperatures start to increase again. At this mass, the footprint of the PS becomes larger than that of the CU and AC.¶¶ As a result, the PS thermal conduction constant $GL_{\mathrm{PS}-X}$ becomes larger than that of the CU and AC, and the temperature of the $-X$ radiator starts to follow that of the PS. This effect then couples back into the CU and AC, and so their temperatures also start to follow those of the PS.

Nonetheless, the main observation is that the subsystem temperatures tend to remain within the typical safe range defined in Sec. III. In other words, whether or not a subsystem reaches a critical temperature does not depend primarily on the downscaling of a satellite.

B. Sensitivity Analysis

1. *Varying Environmental Parameters*

This section presents calculations with orbit parameters other than those used for the standard orbit of Table 1. The first two alternatives are orbits with altitudes corresponding to typical minimum and maximum values. As mentioned in Sec. II, these typical values for LEO missions are 400 and 800 km, with corresponding inclinations of 97.03 and 98.60 deg, respectively. As a third alternative, we have decreased the right ascension of our standard orbit from 98.2 to 90 deg, leaving other parameters unchanged. In such an orbit, the overall environmental heat influx is minimal, whereas it is approximately maximal in our standard orbit. The results of the calculations with these alternative orbits are summarized in Fig. 11, which shows the change in subsystem temperature with respect to the standard orbit plotted against mass. Because the radiator temperatures are mainly affected by the changing environmental influx, the temperature difference is the same for all subsystems mounted on a given radiator panel.

The temperature variation with orbit parameters is relatively insensitive to the satellite mass. Even though different orbits result in different environmental heat fluxes and thus in different satellite and component temperatures, environmental heat exchange remains mass-independent [i.e., Eq. (8) remains valid, albeit with a different prefactor].

It can be further noted that the subsystems on the $-X$ radiator become 15 to 20°C colder when the right ascension is changed to 90 deg. As a result, the PL's temperature tends to fall outside the typical safe range. Although this illustrates how different orbit parameters can lead to undesired temperatures, we stress again that our thermal analysis shows that this is not affected by spacecraft size.

¶¶Note that $A_{\mathrm{PS}-X} > A_{\mathrm{PL}-X}$ throughout the mass range.

2. *Cross-Couplings Between Subsystems*

In the preceding analyses, we assumed that subsystems are thermally connected only indirectly via the radiators. However, when satellites become smaller, radiative coupling terms between subsystems may become significant and may alter the heat balance. To gauge the influence of radiative coupling on subsystem temperatures, we assume such coupling to exist between the PL at the $+X$ radiator and between the other subsystems at the $-X$ radiator. View factors between the subsystems at the $-X$ radiator are considered to be negligible. The exact view factors between the PL at $+X$ and the other subsystems on $-X$ depend strongly on their exact size, shape, and relative position, but can be estimated to range from as low as ∼0.04 to as high as ∼0.3 [11]. Because we cannot pinpoint subsystem shape and relative position in our generalized satellite model, we assume an intermediate view factor of $F_{ij} = 0.1$. We furthermore assume that all subsystems have emissivity $\varepsilon = 1.0$.

In Fig. 12, the resulting subsystem temperatures (dashed lines) are compared with those obtained with the standard analysis (solid lines). Obviously, the temperatures of subsystems mounted on the $-X$ radiator become lower, whereas those at the $+X$ radiator become higher. In other words, the thermal coupling between subsystems tends to homogenize their temperatures. Note further that the mass dependence of the temperatures remains similar to the dependence found in the standard analysis, illustrating once more how the scaling behavior is mainly dictated by heat dissipation in the subsystems.

3. *Footprint of the Battery Pack*

In view of the trend to use smaller components in small satellites, we also analyzed the influence of the PS footprint $A_{\mathrm{PS}-X}$ on the thermal balance. As mentioned in Sec. V.B, this footprint is dominated by the battery pack. Comparing Eqs. (11) and (12), the footprint areas of small-sized batteries tend to be ∼20% smaller than those of average batteries. Because the heat dissipation remains the same, the heat flux from the PS to the $-X$ radiator increases by ∼20%. Assuming that the change in PS footprint has virtually no effect on the other subsystems, the PS temperature increases by about 5°C. It should be noted that this temperature increase may indeed drive the PS in the thermally critical regime (see Fig. 10a).

Obviously, this observation is generally valid for all subsystems: decreasing subsystem size while keeping its heat dissipation level constant will result in an increased heat flux and therefore an increased temperature.

VIII. Conclusions

We analyzed whether or not subsystems in LEO satellites become thermally critical when the satellites become smaller. Assuming typical LEO properties, we defined a generalized model satellite and identified a typical configuration of dissipating subsystems. We then studied the influence of mass scaling on the subsystems' heat

dissipation and on the internal and external thermal couplings. Bringing together this information, mass-scaling trends in the thermal balance of LEO satellites were studied.

Although downscaling does involve different scaling behavior for internal radiative or conductive couplings, the analysis shows that this does not necessarily lead to critical subsystem temperatures. Just as with any satellite, subsystem temperatures are mainly determined by environmental conditions. Furthermore, in lighter satellites, internal radiative coupling becomes significant and subsystem temperatures tend to homogenize. The size of a subsystem relative to its heat dissipation, on the other hand, does constitute a critical factor. When subsystem size reduces faster than its heat dissipation, its temperature may reach critical levels.

Acknowledgments

This work was supported by the Dutch research program for microtechnology, MicroNed. The authors wish to thank E. K. A. Gill, M. Dhallé. and H. Derking for looking over the manuscript.

References

[1] Van Breukelen, E., "Delfi-C3: Delft University of Technology's Nanosatellite," *Proceedings of the 4S Symposium: Small Satellites, Systems and Service* [CD-ROM], ESA Publ. Div., Noordwijk, The Netherlands, Sept. 2006.

[2] Sarda, K., "Canadian Advanced Nanospace Experiment 2: Scientific and Technology Innovation in a Three Kilogram Satellite," *Acta Astronautica*, Vol. 59, No. 1-5, 2006, pp. 236–245. doi:10.1016/j.actaastro.2006.02.054

[3] Narayana, K., "Thermal Design and Performance of HAMSAT," *Acta Astronautica*, Vol. 60, No. 1, Jan. 2007, pp. 7–16. doi:10.1016/j.actaastro.2006.07.001

[4] "Spacecraft Thermal Control Design Data," ESA Rept. PSS-03-108, Vol. 5, Noordwijk, The Netherlands, 1989, Sec. S.

[5] Haimerl, M., "Thermal Control and Design of the ERS-1 Payload," *SAE Technical Paper Series*, Society of Automotive Engineers, Warrendale, PA, 1987, p. 11.

[6] Wertz, J. R., and Larson, W. J., *Space Mission Analysis and Design*, 3rd ed., Kluwer Academic, Dordrecht, The Netherlands, 1999.

[7] Sanders, H. M., "System Analysis and Development of a Cool Gas Generator Based Micropropulsion System," *Proceedings of the 6th Round Table on Micro/Nano Technologies for Space Applications* [CD-ROM], European Space Research and Technology Centre, Noordwijk, The Netherlands, Oct. 2007.

[8] Kayal, H., "BEESAT: A Pico Satellite for the On-Orbit Verification of Micro Wheels," *3rd International Conference on Recent Advances in Space Technologies*, Inst. of Electrical and Electronics Engineers, Piscataway, NJ, June 2007, pp. 497–502. doi:10.1109/RAST.2007.4284041

[9] ESARAD, Software Package, Ver. 6.0.1, Alstom Power Aerospace, Leicester, England, U.K., 2007.

[10] ThermXL, Software Package, Ver. 4.4 b2, Alstom Power Aerospace, Leicester, England, U.K., 2006.

[11] Ehlert, J. R., and Smith, T. F., "View Factors for Perpendicular and Parallel, Rectangular Plates," *Journal of Thermophysics and Heat Transfer*, Vol. 7, No. 1, 1993, pp. 173–174. doi:10.2514/3.11587